Cold Sprayed Cu-MoS_2 and Its Fretting Wear Behavior

Yinyin Zhang[1], Sylvie Descartes[2], Phuong Vo[3], and Richard R. Chromik[1*]

[1]:Department of Mining and Materials Engineering, McGill University, Montreal, QC, H3A 0C5 Canada

[2] :Université de Lyon, CNRS, INSA-Lyon, LaMCoS, UMR5259, F-69621 Villeurbanne, France

[3] :National Research Council Canada, 75, boul. de Mortagne, Boucherville, QC J4B 6Y4, Canada

[*]Corresponding author: Email address: richard.chromik@mcgill.ca (Richard R. Chromik)

Abstract

Cu and Cu-MoS_2 coatings were fabricated by cold spray and the fretting wear performance of the two coatings was compared. A mixture (95 wt.% Cu + 5 wt.% MoS_2) was used as feedstock for the composite coating. Coatings were sprayed with identical gas flow conditions on the substrates preheated to approximately 170°C. The morphology of coating top surface and polished cross sections was analyzed by scanning electron microscopy (SEM) and light optical microscopy (LOM). The influence of MoS_2 on Cu deposition was examined. The local MoS_2 concentration within the coating was found to affect the hardness. Fretting tests were carried out at two different normal loads and the influence of MoS_2 on friction and wear was studied. The morphology and elemental composition of the wear scars and wear debris were observed by SEM and energy dispersive X-ray spectroscopy (EDS), respectively.

Keywords: cold spray; Cu-MoS_2 composite; fretting; wear debris bed; normal load.

1. Introduction

Metal matrix solid lubricant composites are used for engineering parts such as bearings and bushings due to low friction and/or improved wear resistance (Ref 1). They are of particular interest in improving fretting resistance because fretting is a small relative movement occurred between two contacted surfaces and that makes it difficult to provide continuous lubrication by liquid lubricants (Ref 2). For example, Hager Jr. et al. have investigated that nickel graphite composite coatings are able to effectively mitigate fretting damage on titanium alloy compressor blades (Ref 3). Conventional manufacture of such materials includes powder metallurgy, hot pressing, sintering, and thermal spray (Ref 1, 3-8). However, those methods inevitably cause high-temperature-induced decomposition of solid lubricants and/or other phase transformations that could be detrimental for tribological performance (Ref 1, 5,

9). For example, brittle compounds of Cu_2S and $CuMo_2S_3$ were commonly observed in sintered Cu-MoS_2 composites, causing MoS_2 to be ineffective as a solid lubricant and thus resulting in high friction and wear (Ref 5, 9).

In cold spray, particles are accelerated to a high velocity, typically between 500 - 1200 m/s, by use of a de Laval nozzle and a propelling gas that is pressurized and pre-heated to temperatures below the melting temperature of sprayed materials (Ref 10). The formation of dense coatings can thus be mainly attributed to the kinetic energy of particles upon impact, thereby, intrinsically minimizing or eliminating thermally induced chemical changes (Ref 11). This makes it a promising technique for heat sensitive materials such as solid lubricants (Ref 10). Several studies were conducted to fabricate metal-solid lubricant composites by cold spray (Ref 12-14). However, in most cases, pre-treatments on powder such as milling, sintering and particle cladding were required to improve the retention of solid lubricants (Ref 12-14). Therefore, limited research in this field has led to an inadequate understanding on how solid lubricants behave for cold spray.

Fretting is a relative oscillatory motion at a small displacement amplitude which induces harmonic tangential force between two contacting bodies (Ref 15-17). Thus, various surface and subsurface processes are involved in fretting. Generally, for metallic materials, after a small number of cycles, there is a typical four-layer configuration generated: detached particles, which is also called third body (it is defined as the materials generated from the parent materials/first bodies), tribologically transformed structure (TTS) layer, plastically deformed layer, and the base material (Ref 18-21). Third bodies, across which the theoretical velocity difference between first bodies is accommodated, play a critical role in fretting behavior (Ref 20). Within a gross slip regime, where sliding occurs in the entire contact, wear particles are usually generated and trapped within the contact, leading to the rubbing surfaces separated by the wear particles. This situation is called three-body contact. Therefore, sliding induced by fretting is mostly adapted by the third-body behavior. However, in a partial slip regime, where the contact is partially “stuck” together and thus two-body contact plays an important role, fatigue cracks are initiated and become the main material response (Ref 22-23). It is important to note that fretting wear and fretting fatigue can coexist in the same contact if localized two- and three-body contacts are developed simultaneously (Ref 20). Once the contact is completely separated by wear debris bed, further cracking is eliminated (Ref 20, 24). Therefore, well established wear debris bed offers protection on first bodies and decreases fretting damage. Solid lubricants are often used to

lubricate and mitigate fretting wear damage. Generally, they can serve as third bodies that separate the initial contact and protect the first bodies from cracking (Ref 23).

In the present study, the cold spray behavior of MoS_2 and Cu were studied using powders with no pre-treatments. Development of an understanding of how solid lubricants behave in cold spray will serve for future studies in optimizing sprayability and coating properties. For the two coatings, fretting wear tests were conducted and the influence of MoS_2 on friction and wear at different normal loads was studied. Examination of third bodies helped to understand the fretting wear mechanisms for these cold spray coatings and the influence of MoS_2 on these mechanisms.

2. Experimental

A commercially available cold spray system (PCS800, Plasma Giken, Japan) was used to fabricate a Cu and a Cu-MoS_2 composite coatings under the same spraying condition. Spherical Cu powder (Giken, d_{50} = 23 µm) and a flake-like MoS_2 powder (Climax, d_{50} = 30 µm) were used as feedstock (see Fig. 1). The particle size distribution was measured by a laser scattering particle size distribution analyzer (Horiba LA-920). For the composite coatings, a mixture of 95 wt.% Cu and 5 wt.% MoS_2 was mechanically mixed for 1 hour as preliminary study suggests this composition of mixture allows to achieve the best combination of deposition efficiency and MoS_2 retention. Nitrogen was used as the process gas and the gas pressure and preheat temperature were maintained at 5 MPa and 800 °C, respectively. Grit-blasted AA6061 aluminum alloy was used as substrates and were preheated up to around 170 °C immediately before coating deposition by traversing the spray gun over the substrate with the heated gas jet only, i.e., without feeding any powder. Preliminary studies indicated that preheated substrate reduced porosity and enhanced deposition efficiency for the composite coating. Gun traverse speed was set at 60 mm/s, and stand-off distance 40 mm. For observation by light optical microscopy (LOM) and scanning electron microscopy (SEM), cross sections of the coatings were mechanically ground, and polished down to a final step of colloidal silica (0.05 µm). The volume fraction of MoS_2 in the coating was determined by image analysis.

A custom-built fretting device (at Laboratoire de Mécanique des Contacts et des Structures (INSA, Lyon, France)) was used with ball-on-plate configuration, where the upper countersphere is stationary and the lower plate vibrates with small displacement amplitude. In this study, the upper counterspheres are made of AISI 440C steel with a

radius of 50 mm. The lower specimens were AA6061 plates coated with roughly 1 mm thick Cu or Cu-MoS_2. During each test, the normal force, F_n, was kept constant and the tangential force Q and sliding amplitude δ was recorded, which allows plotting fretting loops Q versus δ. The coefficient of friction (CoF) is defined as the ratio of Q/F_n.

In order to eliminate the residual stress induced by a previous machining step, the top surface of the coatings was carefully removed by polishing down to 3 μm diamond suspension. The counterspheres and polished coatings were then ultra-sonic cleaned in an ethanol bath for 15 minutes. The fretting parameters were shown in Table 1. These tests were short, with intention to observe the generation of wear debris bed. Fretting tests were performed in ambient atmosphere at room temperature (20-25°C) with a relative humidity of 35%.

Fretting loops generated from the tests (Fig. 2) were quasi-rectangular, indicating gross slip conditions. For both Cu and Cu-MoS_2, the sliding amplitude, D, was around ±72 μm and ±120 μm, tangential force amplitude Q^*approximately 77 N and 100 N, at 100 N and 150 N normal loads, respectively. The sliding condition was also determined by a non-dimension sliding criterion "A" defined as the ratio of the dissipated energy (E_d) and the total energy of the cycle (E_t), where E_d is the fretting loop area, while $E_t = 4\delta^* Q^*$ (Ref 17). Following this method, the energy ratios of the tests at 100 N and 150 N were calculated as 0.43 and 0.49, respectively. For both coatings at these two normal loads, this was consistent with a gross slip condition (A > 0.2) (Ref 17).

After fretting tests, contacting surfaces of the coatings and counterspheres were examined with a confocal profiler (Altisurf-500), and then observed with a SEM (FEI Quanta 600). Secondary electron (SE) images were taken for morphology observations and energy dispersive X-ray spectroscopy (EDS, oxford instruments) was used for chemical composition analysis.

3. Results

3.1 As sprayed Cu and Cu-MoS_2 coatings

A cross section of the as-sprayed Cu-MoS_2 composite coating shows dark contrast around the splats (Fig. 3a), which was identified as MoS_2 by using EDS mapping (Fig. 3b). The deposition efficiency (DE) of each component was measured as: $DE_{(Cu)}$ = 53%, $DE_{(MoS2)}$= 18.1%, yet the deposition efficiency of pure Cu coating was as high as 97%

with the same spraying parameters. The average MoS_2 concentration was 1.8 ± 1.0 wt.% and was measured from 10 images with a wide range of local MoS_2 concentrations (i.e. regions A and B in Fig. 3a).

As revealed by microhardness tests on regions of varying MoS_2 concentration (Fig. 3c and 3d), higher MoS_2 content led to much lower hardness because of particle de-bonding. This implies that bonding strength between splats was weak due to the presence of MoS_2. Over the range of local MoS_2 concentrations found within the composite coating, combined with the hardness of pure Cu coating, the hardness decreased linearly with MoS_2 concentration (Fig. 4). This demonstrates that the hardness of the composite coating was mainly dependent on MoS_2 content.

Top-down view micrographs (Fig. 5) of the Cu-MoS_2 coating show deep craters that were not observed in the pure Cu coating. Fine MoS_2 fragments were found within the crater (Fig. 5b), indicating MoS_2 particles were fractured upon impact or by the impact of coming Cu particles. The edge of the craters show eroded morphology (Fig. 5c), demonstrating that Cu particles rebounded rather than being deposited due to the presence of MoS_2 fragments. Cross section micrographs of the Cu-MoS_2 coating (Fig. 6) show that MoS_2 is retained at the bottom or side of the splats, noted as white arrows, while the black arrows indicate Cu-Cu contact.

3.2 Fretting behavior of Cu-MoS_2 and Cu coatings

3.2.1. Friction and wear

Plots of the average coefficient of friction (CoF) of Cu-MoS_2 and Cu coatings at 100 N and 150 N (Fig. 7) show that each coating exhibited different behaviors. For both normal loads, Cu-MoS_2 coating was found to have several drops during run-in process, where the friction coefficient fluctuated between roughly 0.4 and 0.54 at 100 N, 0.3 and 0.5 at 150 N. After that, the friction coefficient remained around 0.4. In contrast, Cu coating showed relatively smooth run-in period with no sudden decreases in CoF that was followed by steady state friction coefficient of roughly 0.4.

The wear volumes were measured at the end of the 20,000 and 100,000 cycles for 100 N tests, 10,000 and 30,000 cycles for 150 N tests (Table 2). Both coatings exhibited increased wear volumes with test duration and normal load. For both normal loads, Cu-MoS_2 coating showed higher wear volume at the beginning of the tests compared to Cu. However, with longer test duration, the wear volume of the Cu-MoS_2 was smaller than that of Cu coating for 100 N tests, but was larger than Cu for 150 N tests.

3.2.2. Morphology of worn surfaces

The wear scar of Cu-MoS_2 coating after the 20,000 cycle test at 100 N was mostly covered by wear debris (Fig. 8a-c) with some of the wear debris extruded outside the wear scar. However, in the central region sliding grooves were observed (see Fig. 8b), indicating abrasive wear. A few pits were also found in this area and are indicative of material transfer and wear debris generation. Except for these features, the wear scar was mostly covered by fine wear debris (see Fig. 8c). Similar wear scar morphology was observed for the Cu coating (not shown). The formation of a wear debris bed separates the initial contacting surfaces (first bodies) and the velocity difference during fretting is partly accommodated by motion of the wear debris. This is called three-body contact (see Fig. 8b), while the central transfer region remained two-body contact (see Fig. 8c) (Ref 20).

Similarly, at 150 N, the wear scar of Cu-MoS_2 coating was mostly covered by wear debris (Fig. 9). However, it showed different morphology at the center. As shown in Fig. 9b, a relatively smooth surface with shallow sliding grooves was observed. Cracks, indicated by white arrows, induced by tensile stress were visible. The surface also showed the evidence of some adhesive wear with small tongue-shaped structures, noted as black arrows. The outer region was also covered by a well-established wear debris bed (Fig. 9c). Similar wear scar morphology was also observed for the Cu coating (not shown).

Since generation of wear debris bed changes contact condition and wear mechanism (Ref 20), it is important to examine its development over fretting. As it can be done after a small number of cycles (Ref 18), short tests data was used for analyzing the process. A coverage ratio of wear debris, *c*, shown as equation 1, was used to describe the fraction of the contact that was separated by wear debris.

$$c = \frac{A_{three-body\ contact}}{A_{three-body\ contact} + A_{two-body\ contact}} \qquad \text{(eq1)}$$

Where $A_{three-body\ contact}$ is the area of three-body contact, while $A_{two-body\ contact}$ the area of two-body contact. Table 3 presents coverage ratios of wear debris for both coatings at 20, 000 and 10, 000 cycle tests at 100 N and 150 N, respectively. Cu-MoS_2 coating showed higher coverage ratio at both normal loads, indicating the presence of MoS_2 facilitated generation of the wear debris. In addition, for both coatings, the coverage ratio decreased with normal loads.

Fig. 10 shows morphology of the wear debris outside the wear scars. At 100 N, only fine wear debris were observed for both coatings (Fig. 10a and 10c). However, for Cu-MoS_2 coating, generation of plate-like wear debris up to 200 μm in size was found for 150 N, while compacted fine wear debris was mainly found in Cu coating (Fig. 10b and 10d).

3.2.3. Elemental composition of worn surfaces

Using EDS, elemental composition analysis of the unworn coating and the wear scar revealed increased oxygen in the wear scar. Representative spectra from the regions of interest are shown in Fig. 11, where the relative intensities of Kα peak of oxygen and Lα peak of copper, centered at 0.52 and 0.93 keV, respectively, revealing the different oxygen contents of the unworn coating and the wear scar. In the unworn coating, the copper peak dominated with a small oxygen peak, while at the center of the wear scar, copper intensity remained roughly the same as unworn coating, while oxygen intensity increased. Similarly, a more intense oxygen peak was also found in the outer region of the wear scar as compared to the unworn coating.

Fig. 12 shows elemental composition analysis of the wear debris outside the wear scars for both coatings at 100 N and 150 N. For Cu-MoS_2 coating at 100 N, a higher oxygen peak than that in the unworn coating reveals oxidized wear debris. However, at 150 N, the plate-like wear debris (Fig. 10b) exhibits a low oxygen peak, comparable to the unworn coating. For Cu coating, relatively high oxygen peaks were developed at both normal loads.

4. Discussion

Cold spray was used to fabricate a Cu-MoS_2 composite coating with an average MoS_2 concentration of 1.8 ± 1.0 wt.%, lower than that of the feedstock (5 wt.%). The presence of MoS_2 was also found to significantly decrease the deposition efficiency of Cu to 53% compared to 97% for deposition of Cu alone. MoS_2, due to its nature as a solid lubricant, could potentially inhibit bonding between Cu particles. It exhibits a lamella crystal structure with weak van der Waals forces between the layers, leading to easy shear between planes (Ref 25). The presence of MoS_2 at particle boundaries could inhibit adiabatic shear, which is the main bonding mechanism in cold spray (Ref 11). If MoS_2 is present in regions where normally adiabatic shear between Cu/Cu particles would occur, the shear deformation might instead be accommodated in MoS_2, resulting in a low frictional interface, less temperature rise,

and thus less effective bond. The observation of craters (Fig. 5b) and absence of MoS_2 in regions of adiabatic shear (Fig. 6) and reduction of Cu deposition efficiency with MoS_2 are all consistent with the above explanation of the effect MoS_2 has on cold spray. Fig. 13 shows schematically this process with that flake-like MoS_2 particles were fractured upon impact (step 1). With a high-velocity impact of a Cu particle (step 2), Cu-Cu bonding may occur if the deformation was able to push aside MoS_2 or if the MoS_2 resided in a region away from where adiabatic shear occurs (Fig. 6) (step 3). However, if the MoS_2 resided directly in a region where a Cu-Cu bond is attempted, Cu particles may rebound, causing craters (Fig. 5b). This process should depend on particle velocity and the amount of MoS_2 fragments. The particle velocity should be high enough to push MoS_2 away from the adiabatic shear zone to get strong Cu-Cu bond. On the other hand, the more the MoS_2, the more difficult it would be for Cu deposition. Moreover, even when deposition is achieved, there is a less effective bond between Cu particles in the presence of MoS_2, as was found by the particle de-bonding during hardness measurement and the hardness loss (Fig. 3c and 4).

The fretting behavior of Cu-MoS_2 and Cu coatings was studied under a gross slip regime at normal loads of 100 N and 150 N. For both normal loads, Cu-MoS_2 coating exhibited fluctuation in friction with several sudden drops over run-in period (Fig. 7). That could be due to MoS_2 present at the sliding interface. As discussed above, a solid lubricant provides easy shear and low CoFs. However, since the concentration of MoS_2 within the coating was low (average ~1.8 wt.%) and inhomogeneous (Fig. 3a), MoS_2 could be worn out rapidly and the sliding interface were then mainly controlled by Cu. Even though MoS_2 had an impact on run-in process, the steady-state values, around 0.4, showed no MoS_2 dependence. This could be due to, again, low MoS_2 content. In addition, MoS_2 could be oxidized during the sliding as it was exposed to ambient environment. It may react with H_2O and O_2, resulting in MoO_3 that exhibits poor lubricious property (Ref 16).

Morphology of the wear scars revealed that most of the contacting area had been separated by wear debris even after short tests. That occurred more quickly in Cu-MoS_2 coating, showing higher coverage ratios at both 100 N and 150 N (Table 3). The central transfer region (Fig. 8b and 9b) demonstrated mechanisms of wear particle detachment. At 100 N, abrasion, evidenced by prevailing sliding grooves, was the main mechanism of wear particle generation. However, tensile stress induced cracks were profuse at the wear scar center at 150 N, which could play an important role for wear debris formation (Fig. 9b). In addition, adhesive wear was also found at the central region (Fig. 9b). That was consistent with previous study by Mary et al., where abrasive wear dominates at lower normal force, while

adhesive wear with transfer mechanisms is found to be the main process at higher normal force (Ref 26). Since the wear particles are always much smaller than the contact, they are trapped in the contact, leading to a uniform wear debris bed which separates the initial contact (Ref 20). That process proposed by Berthier et al. interpreted the generation of wear debris bed in the present study. The wear particles also went through considerable changes in elemental composition due to oxidation (Fig. 11 and 12).

Wear debris bed formation changes contact condition and velocity accommodation mechanism (Ref 20). As the contact moved from a two-body (steel against Cu-MoS_2 coating) to a three-body (steel, debris bed and Cu-MoS_2 coating) contact, velocity difference induced by the first bodies was adapted within the debris. That protects the first bodies from high friction, large tensile stresses and subsequent cracking, and therefore makes it fretting resistant (Ref 20, 23). For Cu-MoS_2 coating, due to the relatively weak bonding strength between splats, particle detachment was easier and thus wear debris bed was established faster, that could be another reason for the drops in friction. Low wear after the steady state at 100 N could also be contributed to the protection of wear debris bed. Yet it may cause high wear at the beginning (Table 2). This agrees with the concept of fretting resistant material, where it sacrifices its surface to save its volume (Ref 23).

However, the protection provided by the wear debris bed was not always effective, as evidenced by the higher wear volume of Cu-MoS_2 coating at 150 N (Table 2). This was probably due to the generation of big metallic plate-like wear debris (Fig. 10b and 12b), which is an evidence of severe wear (Ref 27). As they might be too big to be contracted in the contact, they were ejected readily and became bona fide debris, resulting in high wear. Fig. 14 presents schematically the wear scenario of Cu-MoS_2 coating. At lower normal load, an effective debris bed is created that leads to lower wear compared to Cu. However, at a large normal load, e.g. 150 N, and thus a higher friction force, the weak bonds between splats may serve as pre-existing cracks and allow for pulling-off of deformed particles, leading to large metallic wear debris. Ejection of those wear debris develops high wear. In summary, the presence of MoS_2 was twofold. Firstly, it facilitated fast development of wear debris bed, offering protection for the first bodies at low normal load (~100 N). However, at high normal load (~150 N), weak bond between splats caused massive particle detachment and large plate-like wear debris, resulting in high wear.

5. Conclusions

Cu and Cu-MoS_2 coatings were fabricated by cold gas dynamic spray and their fretting behavior were compared. For the cold-sprayed Cu-MoS_2 coating, much less MoS_2 (1.8 wt.%) was retained than in the feedstock (5 wt.%). The presence of MoS_2 inhibited bonding between Cu particles when they were trapped in the region where adiabatic shear normally takes place, leading to a partial bond as well as a decrease in deposition efficiency. For the fretting, the presence of MoS_2 introduced a few drops in CoF during run-in but showed no significant impact on steady state value, which could be due to its low concentration. At the lower normal load tested (100 N) the presence of MoS_2 facilitated fast development of wear debris bed, offering protection for the first bodies and leading to low wear. However, weak bond between splats caused massive particle detachment and large plate-like wear debris and high wear at high normal load of 150 N.

6. Acknowledgements

The authors gratefully acknowledge the financial support from Natural Sciences and Engineering Research Council (NSERC) of Canada. They gratefully acknowledge help from Lisa Lee for data analysis, Walker Nickerson for sample preparation, Lionel Lafarge (INSA-Lyon) for the design of the fretting device, Edouard Régis (INSA-Lyon) for technical help and Tekna Plasma Systems Inc. for donation of the powder. The authors acknowledge administrative support from Drs. Eric Irissou and Jean-Gabriel Legoux (the NRC) and Stephen Yue (McGill University) and technical support from Mr. Jean Francois Alarie at the McGill Aerospace Materials and Alloy Design Center (MAMADC) cold spray facility.

7. References

1. Lansdown, A. R., Tribology Series. Elsevier, Amsterdam (1999)

2. Lancaster J. K., Composite self-lubricating bearing materials, *Proc. Instn. Mech. Engrs.,* 1967-68, **182**(2), pp. 33-54

3. Hager Jr. C.H., et al., The use of nickel graphite composite coatings for the mitigation of gross slip fretting wear on Ti6Al4V interfaces, *Wear*, 2009, **267**, pp. 1470-1481

4. Dhanasekaran, S. et al., Dry sliding friction and wear characteristics of Fe–C–Cu alloy containing molybdenum disulphide, *Mater. Des.*, 2007, **28**, pp. 1135-1141

5. Kato, H. et al., Wear and mechanical properties of sintered copper–tin composites containing graphite or molybdenum disulfide, *Wear*, 2003, **255**, pp. 573-578

6. Du, H. et al., Structure, mechanical and sliding wear properties of WC-Co/MoS2-Ni coatings by detonation gun spray, *Mater. Sci. Eng., A*, 2007, **445-446**, pp. 122-134

7. Du, H. et al., Fabrication and evaluation of D-gun sprayed WC-Co coating with self-lubricating property, *Tribol. Lett.*, 2006, **23**, pp. 261-266

8. Yuan, J. et al., Fabrication and evaluation of atmospheric plasma spraying WC-Co-Cu-MoS2 composite coatings, *J. Alloys Compd.*, 2011, 509, pp. 2576-2581

9. Kovalchenko, A.M. et al., The tribological properties and mechanism of wear of Cu-based sintered powder materials containing molybdenum disulfide and molybdenum diselenite under unlubricated sliding against copper. *Wear*, 2012, **290-291**, pp. 106-123

10. Papyrin, A. et al., Cold Spray Technology, Elsevier, Amsterdam, 2007

11. Assadi, H. et al., Bonding mechanism in cold gas spraying, *Acta Mater.*, 2003, **51** (15), pp. 4379-4394

12. Yamada, M. et al., Fabrication of Cu-MoS_2 composite coating by cold spraying and evaluation of its property, *ITSC 2009: International Thermal Spray Conference*, Las Vegas, 2009

13. Smid, I. et al., Cold-sprayed Ni-hBN self-lubricating coatings, *Tribol.Trans.*, 2012, **55**(5), pp.599-605

14. Aggarwal G., *Ph.D. dissertation*, Development of self-lubricating coatings via cold spray process: Feedstock formulation and deformation modeling, The Pennsylvania State University, (2007)

15. Warmuth, A.R. et al., The effect of contact geometry on fretting wear rates and mechanisms for a high strength steel, *Wear*, 2013, **301**, pp. 491-500

16. Fouvry, S. et al., An effective friction energy density approach to predict solid lubricant friction endurance: Application to fretting wear, *Wear*, 2014, **319**, pp. 211-226

17. Fouvry, S. et al., Analysis of sliding behaviour for fretting loadings: determination of transition criteria, *Wear*, 1995, **185**, pp. 35-46

18. Zhou, Z.R. et al., Nucleation and early growth of tribologically transformed structure (TTS) induced by fretting, *Wear*, 1997, **212**, pp. 50-58

19. Chromik, R.R. et al., Materials phenomena revealed by in situ tribometry, *JOM*, 2012, **64**(1), pp.35-43

20. Berthier, Y. et al., Velocity accommodation in fretting, *Wear*, 1988, **125**, pp. 25-38

21. Sauger, E. et al., Tribologically transformed structure in fretting, *Wear*, 2000, **245**, pp. 39-52

22. Vingsbo, O. et al., On fretting maps, *Wear*, 1988, **126**, pp. 131-147

23. Berthier, Y. et al., Fretting fatigue and fretting wear, *Tribology international*, 1989, **22**(4), pp. 235-242

24. Vincent L., et al., Mechanics and materials in fretting, *Wear*, 1992, **153**, pp. 135-148

25. Savan A., et al., Modern solid lubrication: recent developments and applications of MoS_2, *Lubricant Science*, 2000, **12**(2), pp. 185-203

26. Mary, C. et al., Pressure and temperature effects on fretting wear damage of a Cu–Ni–In plasma coating versus Ti17 titanium alloy contact, *Wear*, 2011, **272**, pp. 18-37

27. Lim S. C., et al., Wear-mechanism maps, *Acta Metall.*, 1987, **35**(1), pp. 1-24

8. Figure captions:

Figure 1: Morphology of as-received powders: (a) Cu, (b) MoS_2.

Figure 2: Typical fretting loops of Cu and Cu-MoS_2 coatings at two different normal loads: (a) 100 N and (b)150 N.

Figure 3: Cross section morphology (a) and chemical composition (b) of the Cu-MoS_2 coating and the microhardness tests (c) (d) on the corresponding regions noted as A and B in (a)

Figure 4: Microhardness varies with MoS_2 concentration: Microhardness linearly decreased with MoS_2 concentration and pure Cu coating shows the highest hardness.

Figure 5: Top-down morphology of Cu-MoS_2 coating. (a): a low magnification image. (b): a high magnification image of the crater, in which fine MoS_2 fragments were found. (c) the edge of the crater, showing eroded morphology.

Figure 6: Cross section of the Cu-MoS_2 coating (a) (b). White arrows indicate where MoS_2 retained while black arrows Cu-Cu contact.

Figure 7: Average CoFs of Cu and Cu-MoS_2 coatings at two different normal loads of 100N and 150N. The arrows indicate drops in CoF in the Cu-MoS_2 coating.

Figure 8: Morphology of Cu-MoS_2 wear scar after 20,000 cycles at 100 N. (a) low magnification image. (b) a close view of rectangle b in (a), showing sliding grooves. The white arrows indicate pits. (c) a close view of rectangle c in (a), exhibiting powdery morphology.

Figure 9: Morphology of Cu-MoS_2 wear scar after 10,000 cycles at 150 N. (a) low magnification image. (b) a close view of rectangle b in (a), showing smooth surface. The white arrows indicate cracks; while black ones tongue-shaped structure. (c) a close view of rectangle c in (a), exhibiting powdery morphology.

Figure 10: Morphology of wear debris outside the wear scars of Cu-MoS_2 coating at 100 N (a) and 150 N (b), Cu coating at 100 N (c) and 150 N (d).

Figure 11: spectra of O Kα and Cu Lα of the interested regions: Unworn Cu-MoS_2 coating, central region (corresponds to Fig. 8b) and outer powdery zone of the Cu-MoS_2 wear scar (corresponds to Fig. 8c) at 100 N after 20,000 cycles.

Figure 12: spectra of O Kα and Cu Lα of wear debris outside the wear scars of Cu-MoS_2 coating at 100 N (a) (corresponds to Fig. 10a) and 150 N (b) (corresponds to Fig. 10b), Cu coating at 100 N (c) (corresponds to Fig. 10c) and 150 N (d) (corresponds to Fig. 10d).

Figure 13: A schematic graph showing how MoS_2 deposited with Cu particles.

Figure 14: A schematic graph of wear scenario of Cu-MoS_2 coating at large normal load.

9. Tables

Table 1 Fretting setup

Normal load (N)	100	150
Imposed slip amplitude (μm)	±110	±220
Frequency (Hz)	10	5
cycles	20,000	10,000

Table 2 Wear volume of Cu and Cu-MoS_2 coatings at 100 N and 150 N

Normal load (N)	100		150	
Cycle number	20,000	100,000	10,000	30,000
Wear volume of Cu ($x10^6$ μm^3)	3.18	24.1	22	88.8
Wear volume of Cu-MoS_2 ($x10^6$ μm^3)	12.3	15.8	45.1	198

Table 3 Coverage ratios of wear debris of Cu and Cu-MoS_2 coatings

Normal load (N)	100	150
Cycle number	20,000	10,000

Coverage ratio for Cu coating (%)	89.6	75.7
Coverage ratio for Cu-MoS_2 coating (%)	94.4	90.7

Fig. 1

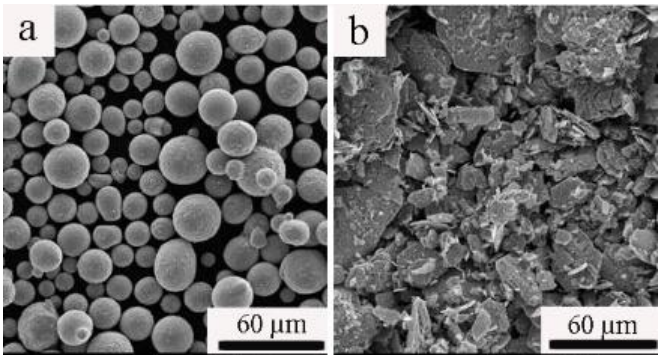

Fig. 2

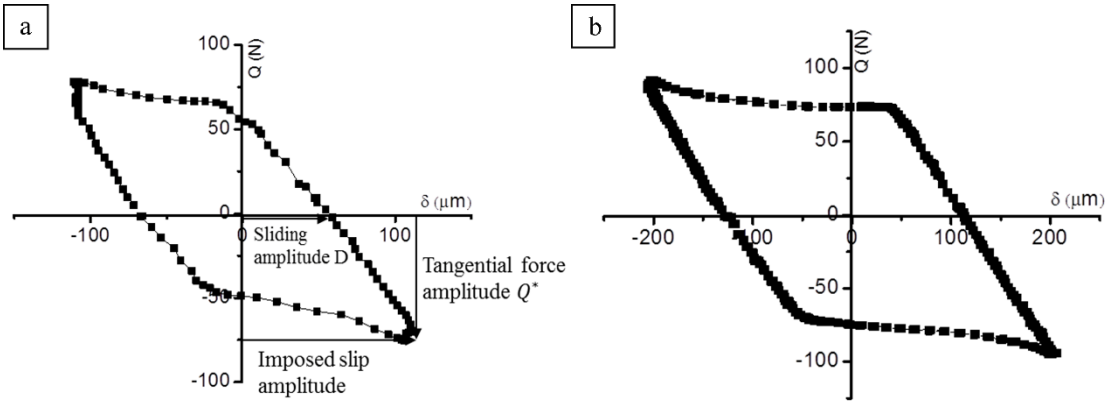

Fig. 3

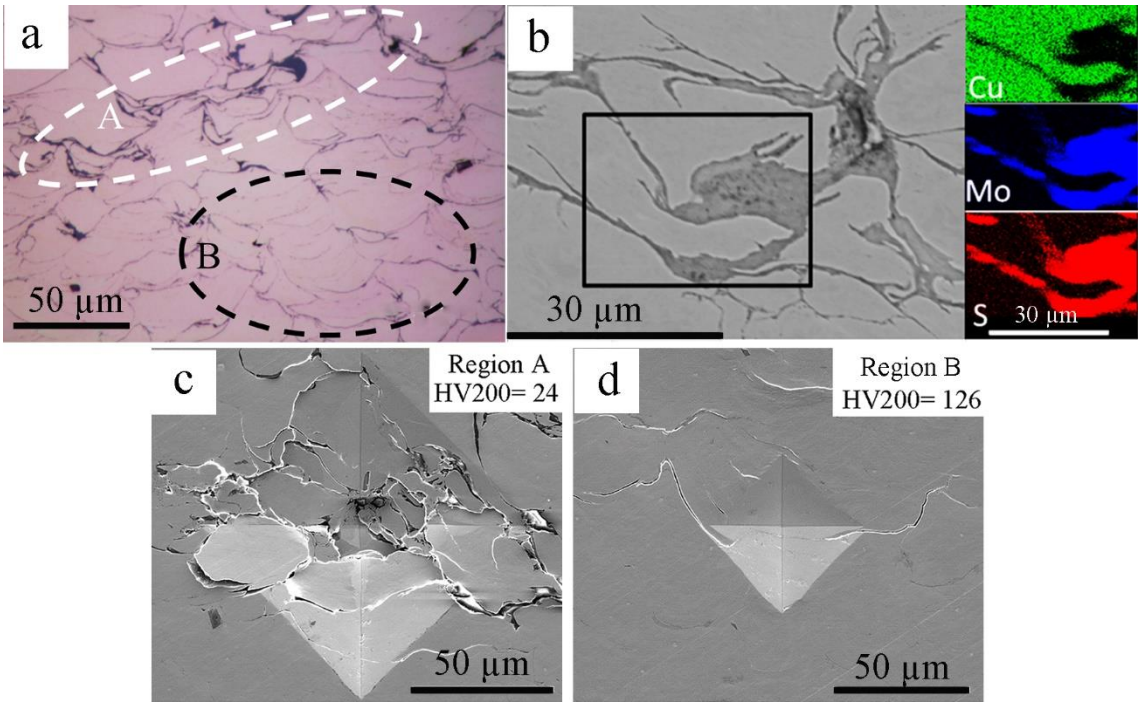
a
A
B
50 µm
b
30 µm
Cu
Mo
S
30 µm
c
Region A
HV200= 24
50 µm
d
Region B
HV200= 126
50 µm

Fig. 4

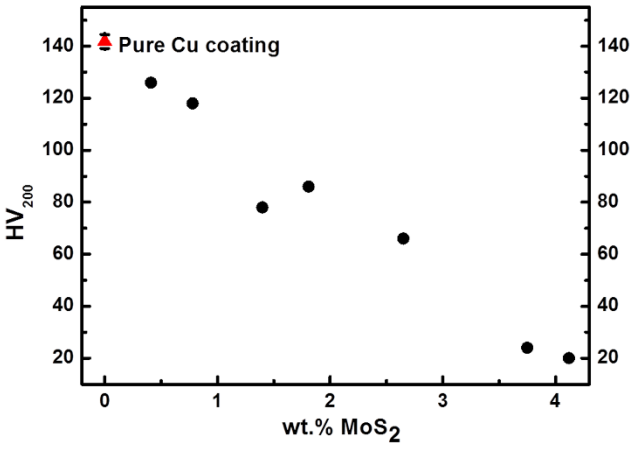
Pure Cu coating
HV200
wt.% MoS2
140
120
100
80
60
40
20
0
1
2
3
4

Fig. 5

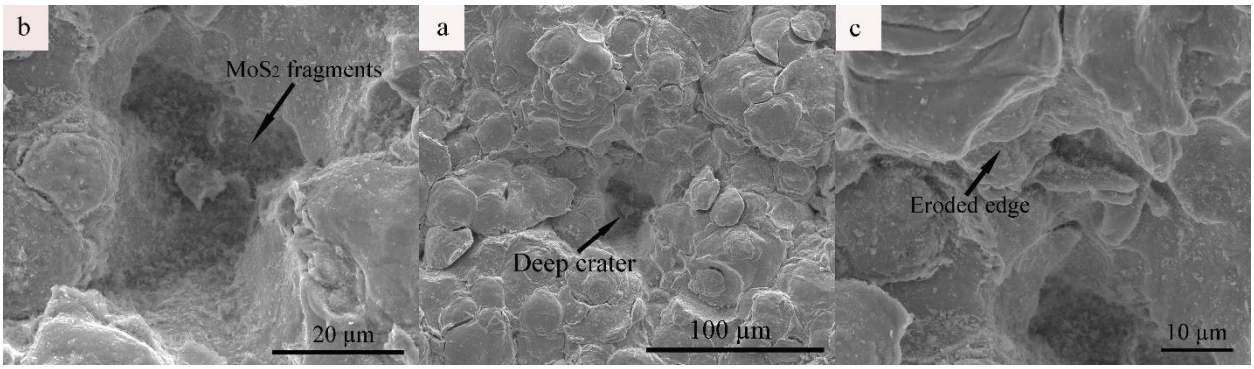
b
MoS2 fragments
20 µm
a
Deep crater
100 µm
c
Eroded edge
10 µm

Fig. 6

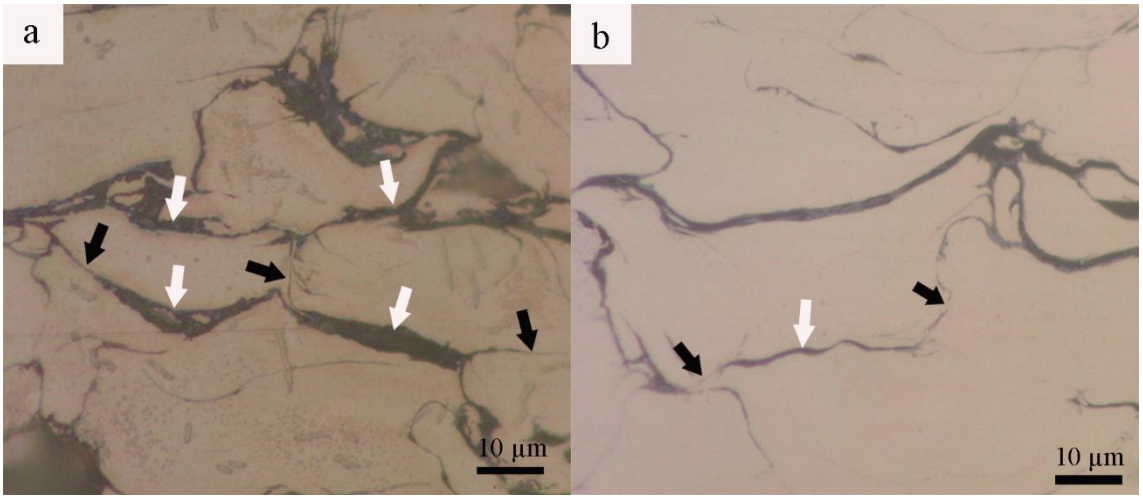
a
10 µm
b
10 µm

Fig. 7

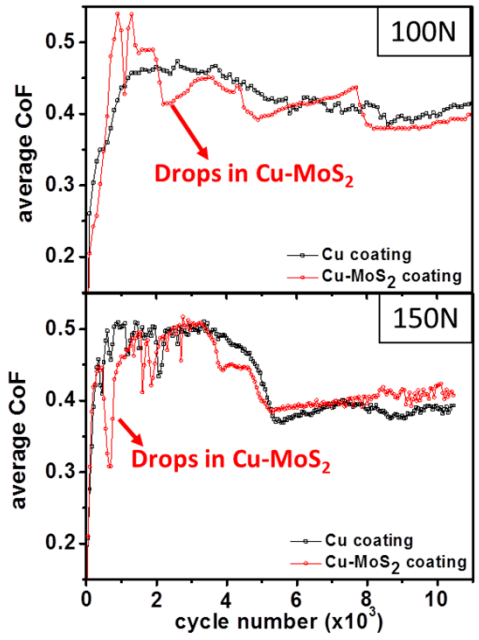
100N
average CoF
Drops in Cu-MoS2
Cu coating
Cu-MoS2 coating
150N
average CoF
Drops in Cu-MoS2
Cu coating
Cu-MoS2 coating
cycle number (x10^3)

Fig. 8

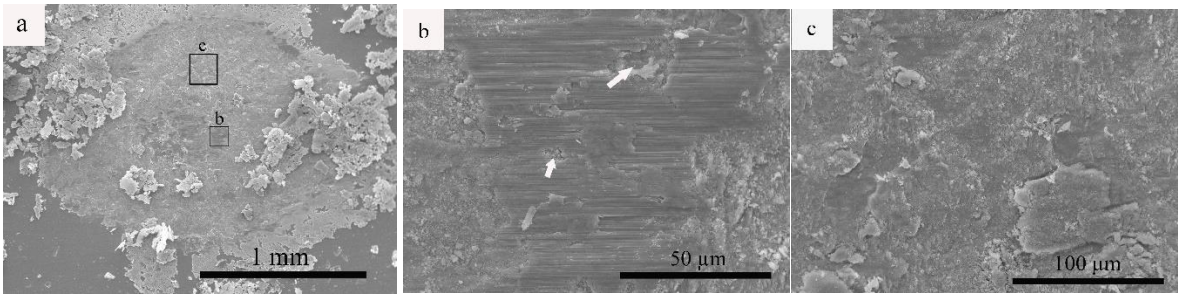

Fig. 9

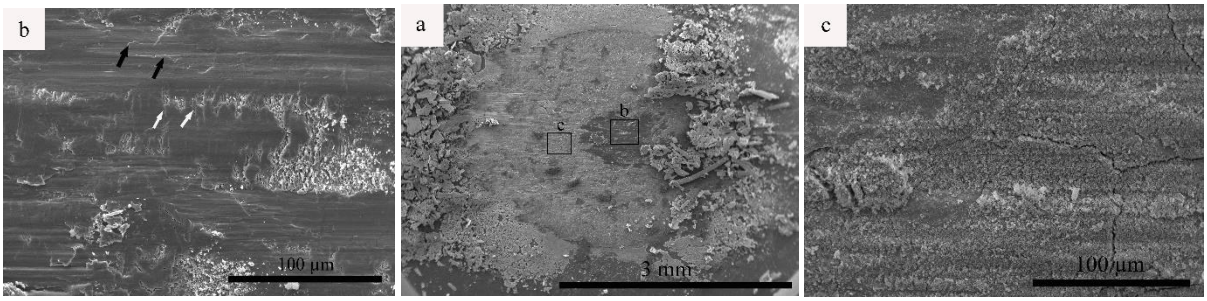

Fig. 10

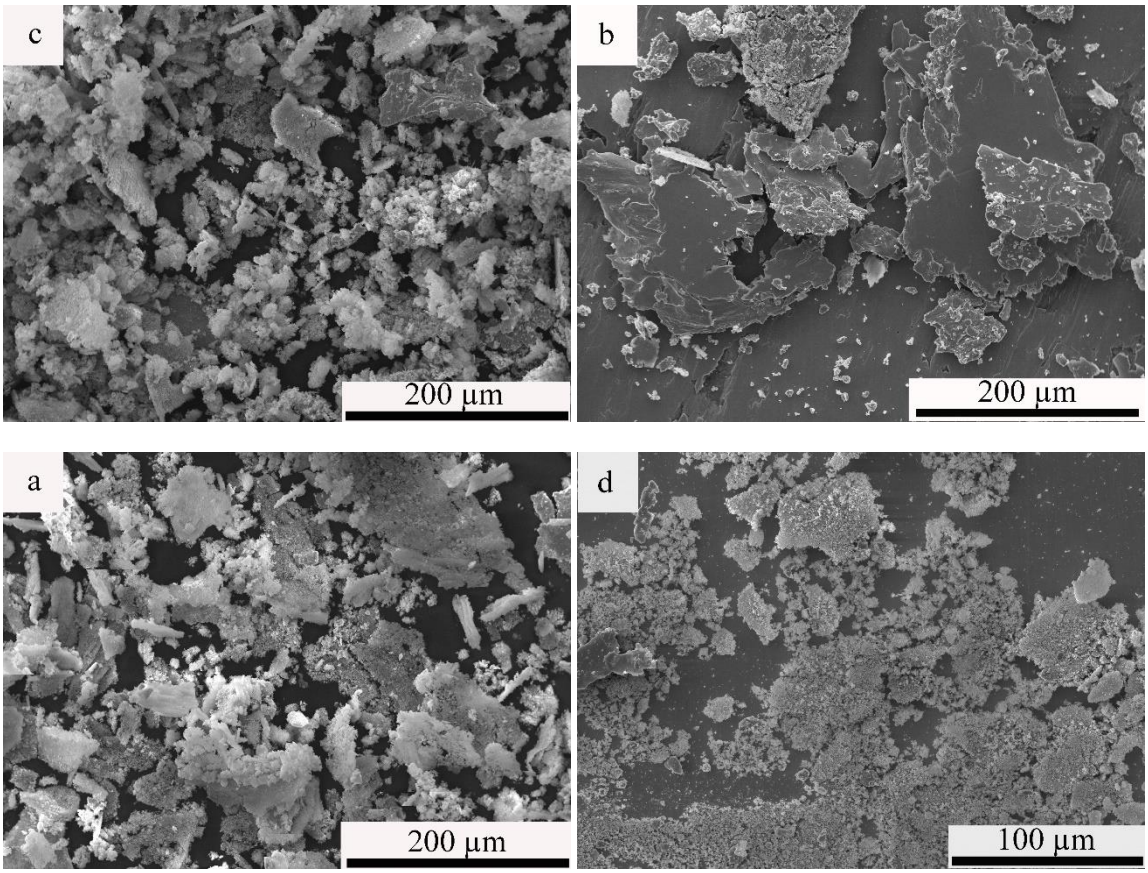

Fig. 11

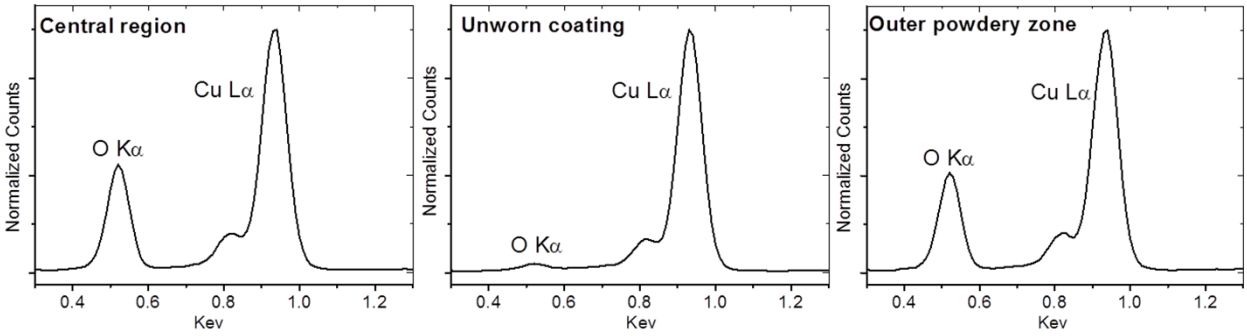

Fig. 12

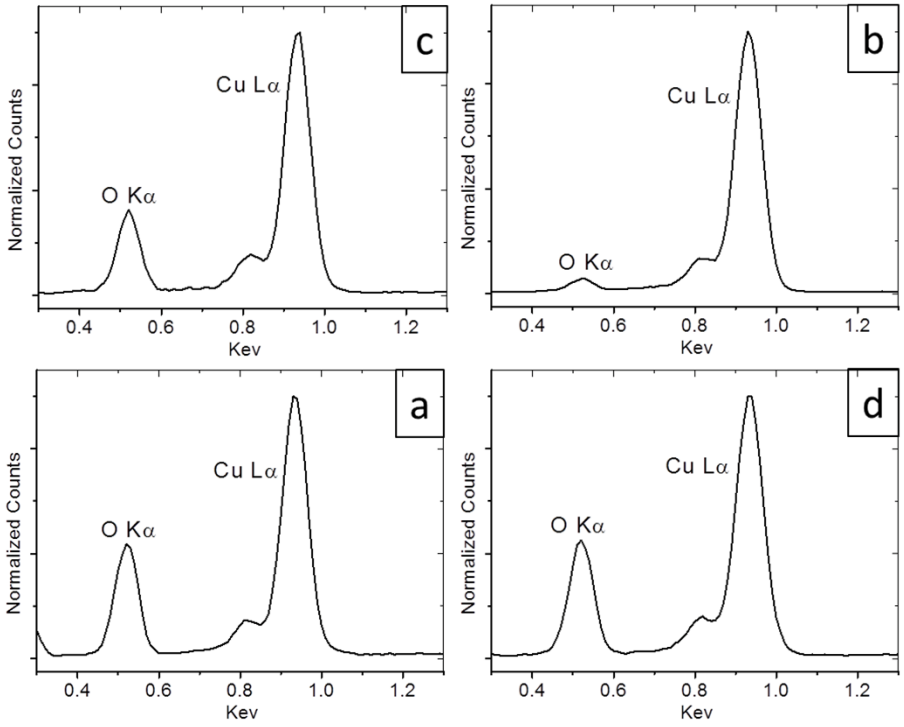

Fig. 13

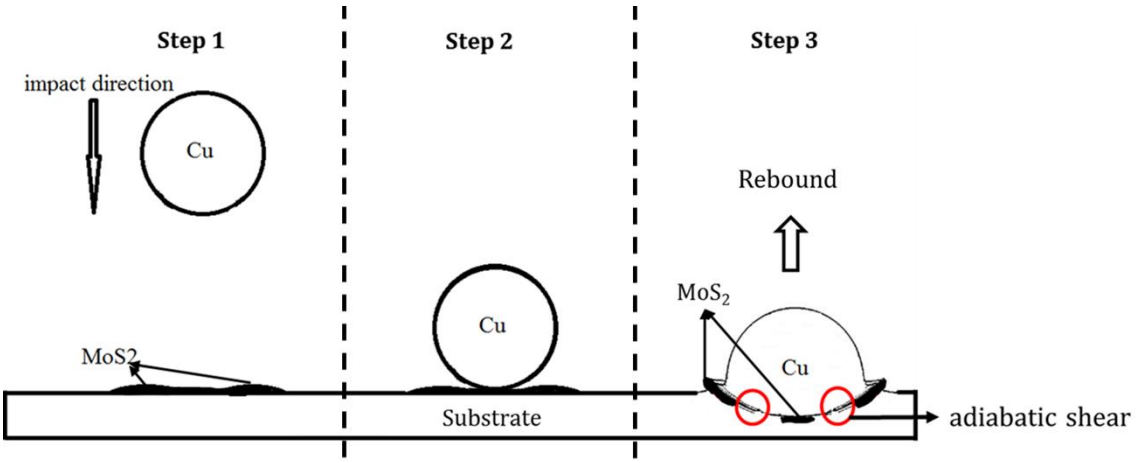
Step 1
Step 2
Step 3
impact direction
Cu
Rebound
MoS2
Cu
MoS2
Cu
Substrate
adiabatic shear

Fig. 14

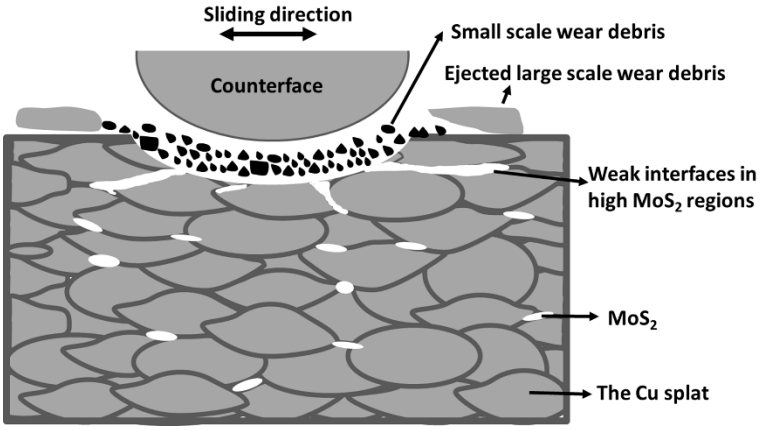
Sliding direction
Small scale wear debris
Counterface
Ejected large scale wear debris
Weak interfaces in high MoS2 regions
MoS2
The Cu splat